ACS OMEGA

Open Access

http://pubs.acs.org/journal/acsodf

Article

Carbon Nanotube-Supported Bimetallic Core–Shell (M@Pd/CNT (M: Zn, Mn, Ag, Co, V, Ni)) Cathode Catalysts for H_2O_2 Fuel Cells

Burak Yapici and Ozlem Gokdogan Sahin*

Cite This: *ACS Omega* 2023, 8, 38577−38586

Read Online

ACCESS | Metrics & More | Article Recommendations

ABSTRACT: M@Pd/CNT (M: Zn, Mn, Ag, Co, V, Ni) core−shell and Pd/CNT nanoparticles were prepared by sodium borohydride reduction and explored as cathode catalysts for the hydrogen peroxide reduction reaction. Electrochemical and physical characterization techniques are applied to explore the characteristics of the produced electrocatalysts. The cyclic voltammetry (CV) experiments show that Zn@Pd/CNT-modified electrodes have a current density of 273.2 mA cm^{-2}, which is 3.95 times higher than that of Pd/CNT. According to the chronoamperometric curves, Zn@Pd/CNT has the highest steady-state current density for the H_2O_2 electro-reduction process among the synthesized electrocatalysts. Moreover, electrochemical impedance spectroscopy (EIS) spectra confirmed the previous electrochemical results due to the lowest charge transfer resistance (35 Ω) with respect to other electrocatalysts.

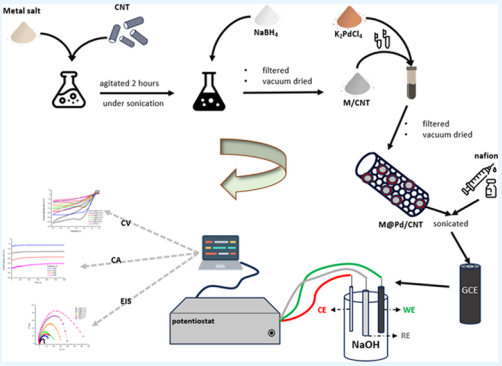

1. INTRODUCTION

Fuel cells have gained much attention as effective and clean energy devices. They are emerging as prime energy transformation ways for several areas in fixed and mobile applications.[1] However, price is a big barrier interrupting fuel cell distribution because of the requirement of a high loading of noble metals such as platinum.[2] The cost can be reduced meaningfully by using alternative noble metals.[3,4]

Benchmarked with liquid fuels, hydrogen peroxide (H_2O_2) is a promising liquid fuel consisting of hydrogen and oxygen.[5] H_2O_2 fuel cells have been receiving growing consideration due to their high energy density and cell potential. Hydrogen peroxide fuel cells have the benefits of no side products and, therefore, no poisoning of the modified electrodes.[6] In addition, the H_2O_2 reduction reaction with two electrons has better kinetics than O_2 reduction to H_2O_2 with four electrons.[7,8] H_2O_2 can be used in a H_2O_2 fuel cell system in two ways, i.e., as a fuel or oxidant, and it can be constructed according to its usage.[9]

The superiority of H_2O_2 reduction has an outstanding influence on the execution of H_2O_2 fuel cell behaviors. Moreover, liquid H_2O_2 has the benefits of suitable carriage and storage for both space crafts and submarines. Concurrently, electro-reduction of H_2O_2 takes place in the two-phase boundary, which is more achievable than the reduction of O_2 electro-reduction taking place in a three-phase zone.[10] As a consequence of the above properties, H_2O_2 is an impressive substitute for O_2 in fuel cells.[11] The reduction of H_2O_2 is executed with the subsequent reaction (eq 1) in an alkaline medium

$$HO_2^- + H_2O + 2e^- \rightarrow 3OH^- E^0 = 0.87\ V \quad (1)$$

Over the past few years, crucial attempts have been made to improve the electrode modification to improve the electron transfer effectiveness, which is extremely related to fuel cells' performances. Among these above-mentioned options for the applications of fuel cells, electrode modification has a great effect on electron transfer.[12]

Currently, noble metals, transition metals, metal oxides, and metal and organic compound mixtures are the main electrode materials used in H_2O_2 reduction.[13−15] Among these, Pd as the illustrative noble metal is usually taken into consideration to improve catalyst activity, since it has the same features as Pt, but it is more abundant and cheaper. Considering both metals present the same conformation,[9,16] Pd can be used instead of Pt due to its high electron utilization rate and adsorption capacity.[17] Moreover, Pd could encourage the breaking of O−O bonds in H_2O_2.[11] However, the main drawback in the design of fuel cells is the cost of the precious metals used for catalyst manufacturing. This problem will be solved by developing high-performance and low-price electrode catalysts. Therefore, researchers have concentrated on adding less expensive metals into Pd catalysts to increase the catalytic activity and reduce

Received: July 28, 2023
Accepted: September 25, 2023
Published: October 2, 2023

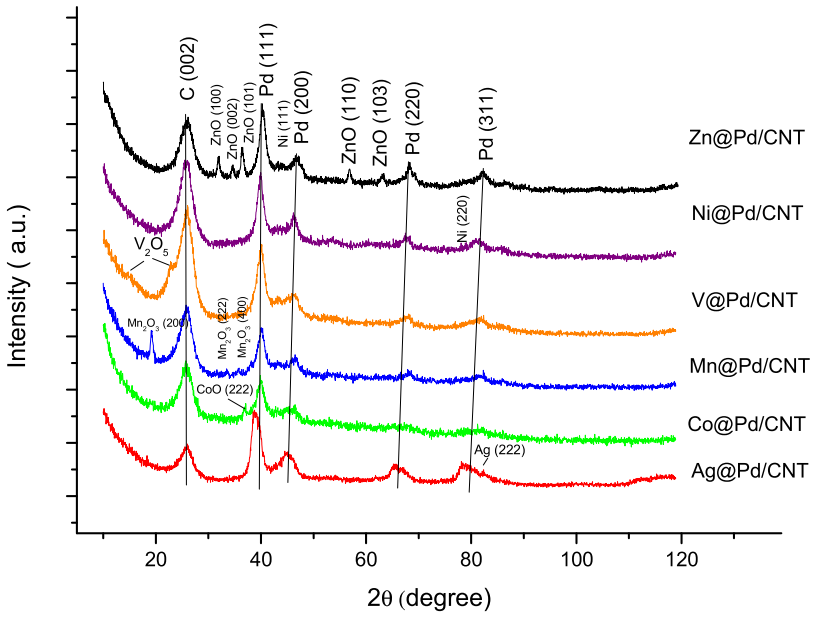

Figure 1. XRD graphs of the M@Pd/CNT nanoparticles.

the cost of Pd metal by exploiting the structure, electronic, and synergistic effects among different materials. Literature studies[7,15,16,18] have confirmed that owing to synergistic catalytic outcomes, bimetallic catalysts express higher catalytic activity than any single one.[19] According to research by Sun et al.,[20] Cu in the PdCu/C electrode enters the Pd lattice and modifies its electronic structure, giving the hydrogen peroxide reduction reaction better performance than commercial Pd/C. For instance, because of the strong electronegativity of Au and the synergistic interaction between Pd and Au, the catalytic performance of the electro-reduction of H_2O_2 might be enhanced by doping the Pd electrode with a second metal of Au.[21]

Typically, the core−shell form has an efficient morphology for increasing catalytic activity. These nanoparticles are commonly preferred to alloy nanoparticles due to the improvement in the usage level of a noble metal at the external surface.[22] Otherwise, the core and shell structure decreases the load of the metal and increases its impact.[23,24] This structure can exhibit the effects of synergistic between the core and the shell that improves the electrochemical reaction activity.[25] Besides, the activity of the core−shell structure is related to the underlying interface between the core and shell metals due to the bimetallic mechanism.

As noble metals employed in catalyst synthesis are expensive, support materials are used to moderate the cost. Catalysts are dispersed over the support materials rather than being used as one piece, reducing the load of the catalyst used and increasing the catalyst surface area.[26] Besides that, the support materials used together with the catalyst can enhance the catalytic activity.[27] Carbon-supported materials such as graphene, graphene oxides, and carbon nanotubes have higher activity and stability than unsupported metal catalysts.[28] With their benefits of a high specific surface area, good chemical stability, low resistance, thermal stability, great flexibility, and superior electrical properties, carbon nanotubes (CNTs) are a common choice for electrode materials.[29]

In this paper, the $NaBH_4$ reduction method was used to create M@Pd/CNT (M: Zn, Mn, Ag, Co, V, Ni) and Pd/CNT. The structural, morphological, and electrochemical features of the prepared materials were characterized. Using a three-electrode setup, the behavior of the catalysts regarding the hydrogen peroxide reduction reaction was studied with electrochemical procedures. Also, the impact of experimental conditions on the catalytic activity of electrocatalysts was evaluated.

2. EXPERIMENTAL SECTION

2.1. Apparatus. A CHI660E potentiostat device was used for electrochemical measurements. The electrode cleaning and dispersion processes by adding Nafion to catalyst powders were carried out in a Branson 1510-MTH ultrasonic bath. A Scilogex MS−H-S was used as a magnetic stirrer.

2.2. Chemicals. Sodium hydroxide (NaOH) and hydrogen peroxide (H_2O_2) were used in the experimental studies. Ethanol (C_2H_5OH) and alumina powder (Al_2O_3) were used to clean the working electrodes. In the catalyst preparation stage, palladium(II) chloride ($PdCl_2$), manganese(II) chloride ($MnCl_2$), silver nitrate ($AgNO_3$), cobalt chloride ($CoCl_2$), zinc chloride ($ZnCl_2$), vanadium(V) oxide (V_2O_5), nickel(II) sulfate ($NiSO_4$), sodium borohydride ($NaBH_4$), carbon nanotubes (CNT), and Nafion solution were used and obtained from Alfa Aesar.

2.3. Catalyst Preparation. Bimetallic core−shell catalysts with 10% Pd content were obtained using the $NaBH_4$ reduction technique. In order to synthesize M/CNT, an appropriate quantity of $ZnCl_2$, $MnCl_2$, $AgNO_3$, $CoCl_2$, VCl_3, and $NiSO_4$ solutions was prepared in water first. The solution was then agitated for 2 h while the CNT support material was added under sonication. A certain quantity of $NaBH_4$ was mixed to obtain M/CNT nanoparticles. Then, it was filtered, cleaned, and vacuum-dried at 90 °C for 14 h. A suitable quantity of M/CNT nanoparticles and K_2PdCl_4 was added to water to synthesize bimetallic M@Pd/CNT (M: Zn, Mn, Ag, Co, V, Ni) catalysts.

2.4. Catalyst Characterization. M@Pd/CNT and Pd/CNT nanoparticles were characterized by using X-ray diffraction (XRD) investigations. The crystallographic struc-

https://doi.org/10.1021/acsomega.3c05531
ACS Omega 2023, 8, 38577−38586

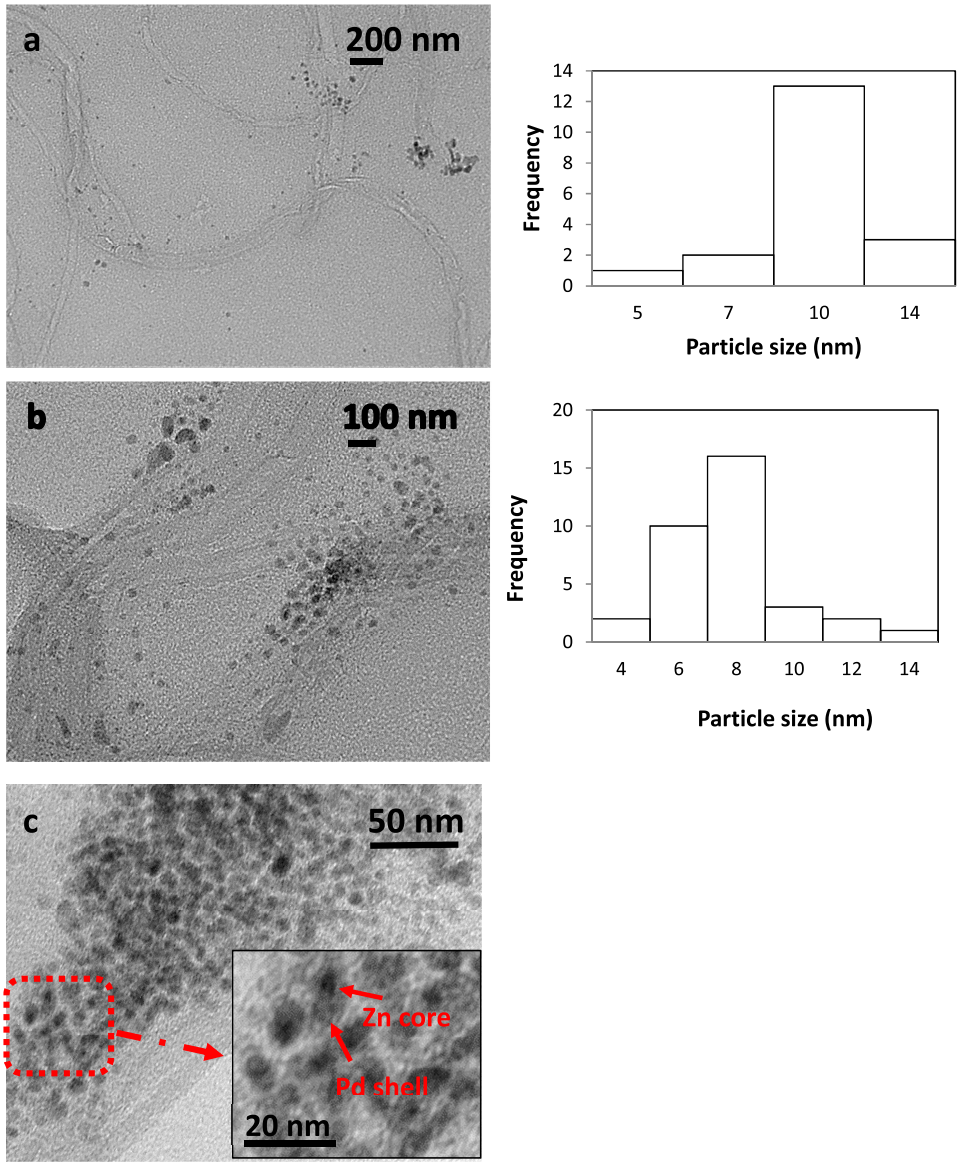

Figure 2. TEM images of the Zn@Pd/CNT catalyst at (a) 200, (b) 100, and (c) 50 and 20 nm.

ture of these catalysts was examined with XRD. The particle crystallite size was obtained from Scherrer equality. The morphology and particle dimensions were examined by transmission electron microscopy (TEM) (Zeiss Sigma 300) operating at 200 kV. The Specs-Flex gadget used X-ray photoelectron spectroscopy (XPS) analysis to detect the oxidation status of the Zn@Pd/CNT catalyst.

2.5. Electrode Modification. The prepared solid catalyst was spread in Nafion solution. Catalyst inks were obtained by an ultrasonic bath for 30 min. 3 μL was taken from the catalyst ink with the help of a micropipette, then applied on the working electrode surface, and dried.

2.6. Electrochemical Analysis. Using a potentiostat (CHI660E) linked to a computer, cyclic voltammetry (CV), chronoamperometric (CA), and electrochemical impedance spectroscopy (EIS) experiments were conducted in an electrochemical cell with three electrodes such as Ag/AgCl reference, GCE working, and Pt wire counter electrodes. The working electrode was cleaned with alumina powder and ethanol after each measurement.

3. RESULTS AND DISCUSSION

3.1. Physicochemical Characterization. The XRD spectra of M@Pd/CNT catalysts are listed in Figure 1. All of the catalysts showed a wide peak at about 26° relative to the hexagonal (002) carbon plane (JCPDS card no. 75-1621). Furthermore, the XRD findings of the catalysts revealed the (111), (200), (220), and (311) planes, confirming the Pd face-centered cubic (fcc) crystalline structure (JCPDS card no. 46-1043). Diffraction peaks appearing in the pattern of the Zn@Pd/CNT catalyst at 2θ values of 32.0, 33.2, 36.6, 40.26, 47.1, 56.7, 63.0, and 68.3° were assigned to ZnO(100), ZnO(002), ZnO(101), Pd(111), Pd(200), ZnO(110), ZnO(103), and Pd(220), respectively. The Co@Pd/CNT catalyst exhibited diffraction peaks at 36.9, 40.23, 46.6, 65.6, and 81.3° corresponding to the CoO(222), Pd(111), Pd(200), Pd(220), and Pd(311) planes, respectively. Furthermore, low-intensity PdO peaks were observed. The Mn@Pd/CNT catalyst's diffraction peaks at 19, 31, 36, and 41° can be attributed to Mn_2O_3(200), Mn_2O_3(222), and Mn_2O_3(400) (JCPDS card no. 24-0508). Low-intensity PdO peaks were

https://doi.org/10.1021/acsomega.3c05531
ACS Omega 2023, 8, 38577−38586

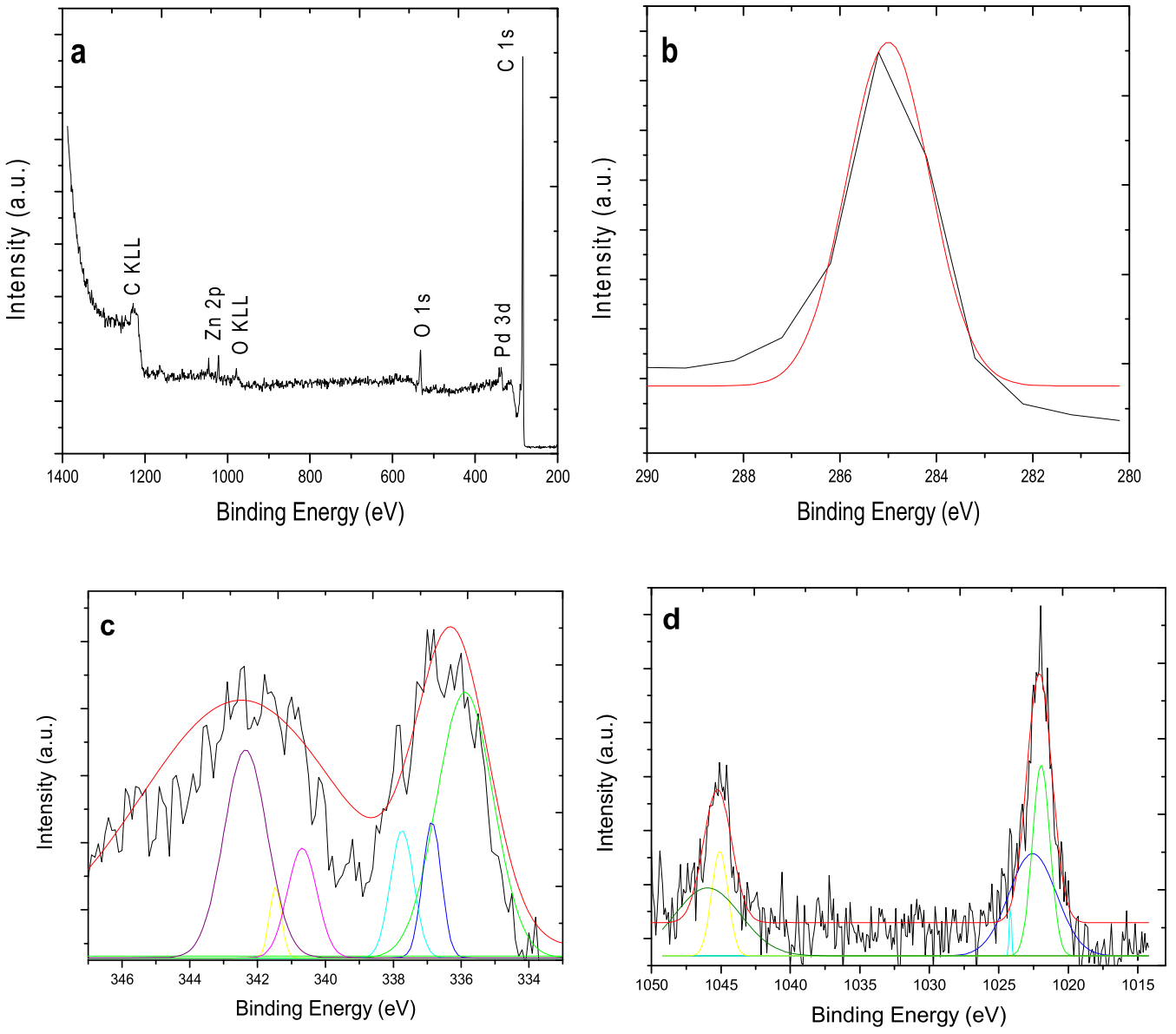

Figure 3. Spectrum of (a) general, (b) C 1s, (c) Pd 3d, and (d) Zn 2p of the Zn@Pd/CNT catalyst.

identified at 43.5, 51.2, and 60.2°. From the XRD analysis of V@Pd/CNT, VO_2 and V_2O_5 peaks are observed, except for the Pd and PdO peaks. The diffraction peaks at 37.9, 43.4, 65.1, 65.9, 78.1, 79.4, and 81.7° of the Ag@Pd/CNT catalyst were attributed to Pd(111), Pd(200), Ag(220), Pd(220), Ag(311), Pd(311), and Ag(222), respectively (JCPDS card no. 04-0783). The XRD pattern of Ni@Pd/CNT showed (111) (44.2°), (200) (52.9°), and (220) (78.8°) peaks. The crystallite size of M@Pd/CNT (M: Zn, Mn, Co, Ag, V, Ni) catalysts was calculated to be 5.50, 5.40, 6.51, 6.52, 6.96, and 7.00 nm, respectively, using the Scherrer equation.

The TEM analysis of the Zn@Pd/CNT catalyst at different scales and the graphs of particle size distribution are presented in Figure 2a,2b. The inset of Figure 2c shows that Zn nanoparticles have a black core and Pd nanoparticles have a bright shell, representing the formation of core−shell nanostructures. As seen in the figure, metal nanoparticles show a regular distribution on the CNTs. From the ImageJ program, the average particle size of Zn@Pd/CNT was found to be 7.7 nm.

Following that, the oxidation states of the Zn@Pd/CNT catalyst were determined by XPS. Zn@Pd/CNT total spectra revealed C 1s, O 1s, Pd 3d, and Zn 2p peaks (Figure 3a). Figure 3b shows the binding energy of C 1s. The spectra of Pd 3d in Figure 3c could be ascribed to Pd^0 (at 334.8 and 341.6 eV), PdO (at 342.2 eV), $Pd(OH)_x$ (at 336.4 and 340.9 eV), and PdO_2 (at 337.6 eV). Furthermore, the spectra of Zn 2p at 1022.1 and 1045.2 eV demonstrated that Zn was mostly present as Zn^{2+} (Figure 3d). In addition, the uncurved peak at 1023.1 eV is considered to be $Zn(OH)_2$. The Zn@Pd core−shell had a greater Pd concentration, suggesting that Pd was mostly dispersed in the outer layer shell.

3.2. Electrochemical Characterization. Figure 4 shows the CV curves of M@Pd/CNT (M: Zn, Mn, Ag, Co, V, and Ni) and Pd/CNT-modified glassy carbon electrodes in a 1.0 M N_2-saturated sodium hydroxide electrolyte solution. The modified electrodes have shown the common behavior of palladium-based catalysts in an alkaline medium.[30−32] The peaks between −1.1 and −0.6 V are attributed to the hydrogen adsorption/desorption on palladium, while the prominent

https://doi.org/10.1021/acsomega.3c05531
ACS Omega 2023, 8, 38577−38586

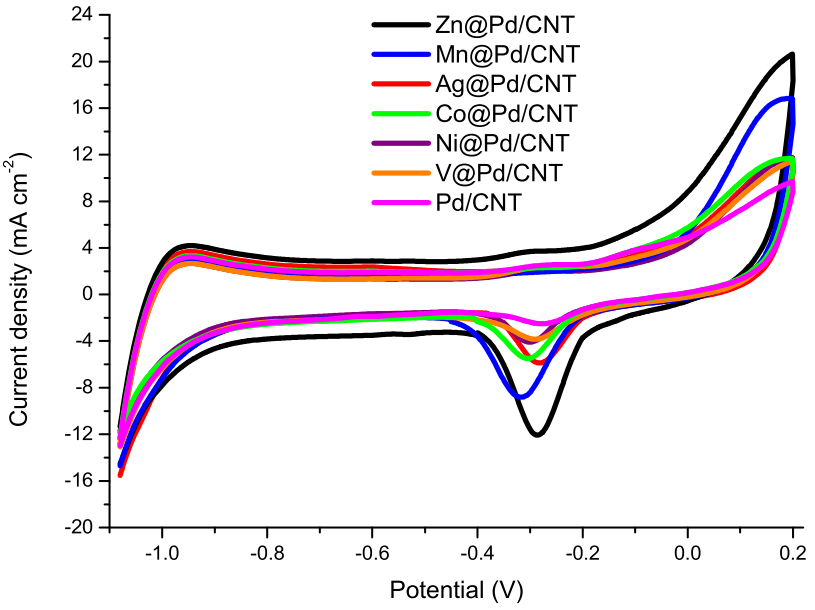

Figure 4. Cyclic voltammograms of M@Pd/CNT (M: Zn, Mn, Ag, Co, V, and Ni) and Pd/CNT-modified GCEs in 1.0 M NaOH at 20 mV s^{-1}.

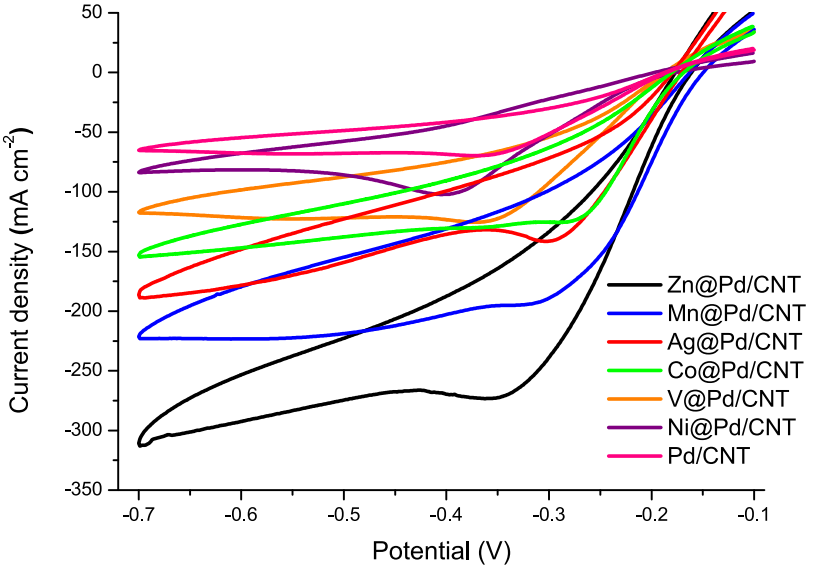

Figure 5. Cyclic voltammograms of M@Pd/CNT- (M: Zn, Mn, Ag, Co, V, Ni) and Pd/CNT-modified GCEs in 0.25 M H_2O_2 + 1.0 M NaOH at 20 mV s^{-1}.

cathodic peaks typical of palladium oxides are between −0.45 and −0.05 V in the back scan, which is generally employed to calculate the catalysts' electrochemical surface areas (ECSAs, eq 2)

$$\text{ECSA} = Q/(0.405 \times \text{Pd}) \quad (2)$$

where Q is the consumed charge for PdO reduction on the modified electrode, and the needed charge for PdO reduction is 0.405 mC cm^{-2}.[23,31,33] The ECSA values of Zn@Pd/CNT (22.1 m^2 g^{-1}) are 4.70, 3.81, 2.95, 1.88, 1.65, and 1.12 times higher than Pd/CNT (4.7 m^2 g^{-1}), Ni@Pd/CNT (5.8 m^2 g^{-1}), V@Pd/CNT (7.5 m^2 g^{-1}), Co@Pd/CNT (11.6 m^2 g^{-1}), Ag@Pd/CNT (13.4 m^2 g^{-1}), and Mn@Pd/CNT (19.8 m^2 g^{-1}), respectively. The greater area for Zn@Pd/CNT supports improved electrochemical activity and Pd consumption in an alkaline medium compared to other produced catalysts.

The cyclic voltammograms of M@Pd/CNT (M: Zn, Mn, Ag, Co, V, Ni) and Pd/CNT-modified GCE were obtained in the potentials varying from −0.1 to −0.7 V. Without H_2O_2, no recognizable change in current was detected over the full potential range, indicating that no distinguishable activity occurred on the electrode surface. However, the cathodic scan at around −0.3 V, which represents the H_2O_2 reduction that follows a two-proton and two-electron reaction, showed a substantial rise in the response after the H_2O_2 addition to the solution (eq 3).[34]

$$H_2O_2 + 2H^+ + 2e^- \rightarrow 2H_2O \quad (3)$$

As shown in Figure 5, the current density of hydrogen peroxide reduction on Zn@Pd/CNT (273.2 mA cm^{-2}) is 3.95, 2.68, 2.27, 2.18, 1.93, and 1.41 times higher than those on Pd/CNT (69.2 mA cm^{-2}), Ni@Pd/CNT (102.1 mA cm^{-2}), V@Pd/CNT (120.3 mA cm^{-2}), Co@Pd/CNT (125.6 mA cm^{-2}),

https://doi.org/10.1021/acsomega.3c05531
ACS Omega 2023, 8, 38577−38586

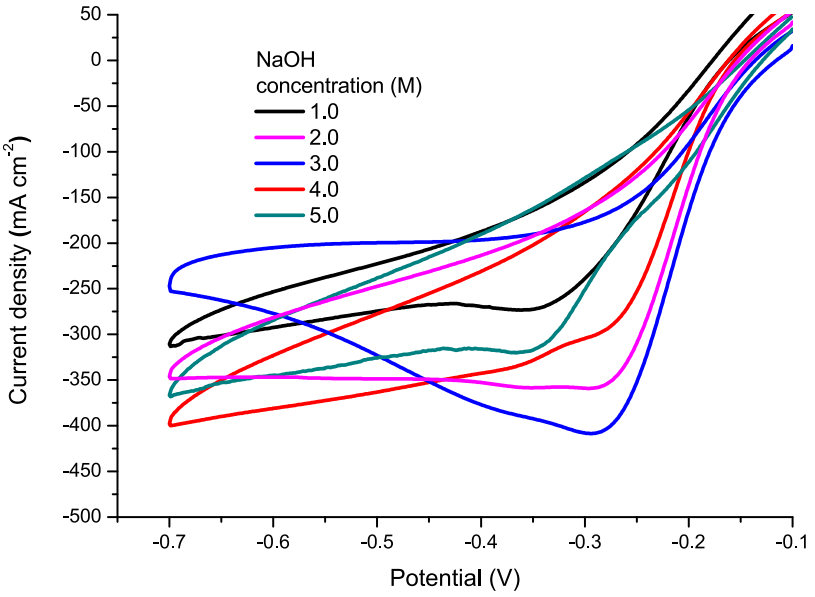

Figure 6. Cyclic voltammograms of Zn@Pd/CNT-modified GCEs at different concentrations (1.0−5.0 M) of sodium hydroxide and 0.25 M hydrogen peroxide.

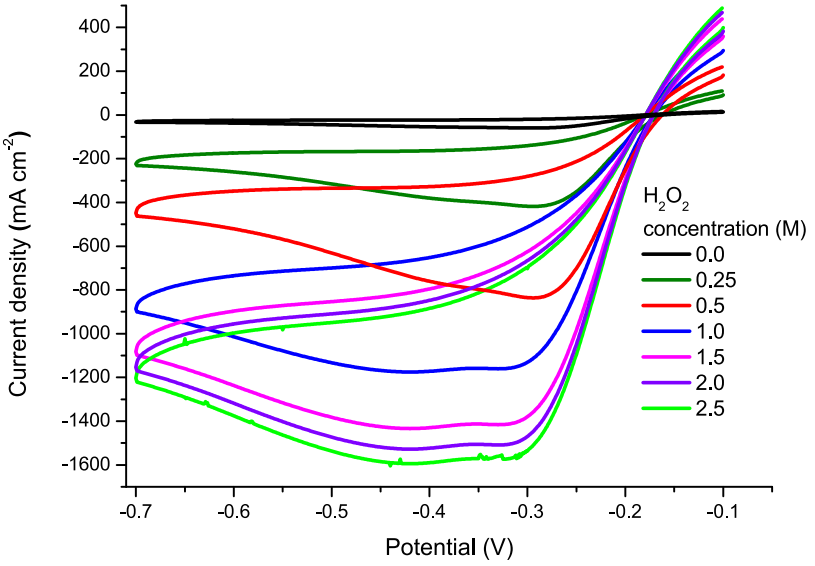

Figure 7. Cyclic voltammograms recorded on Zn@Pd/CNT-modified GCE in a 3.0 M NaOH solution at different concentrations of H_2O_2 (0.0−2.5 M).

Ag@Pd/CNT (141.5 mA cm^{-2}), and Mn@Pd/CNT (193.4 mA cm^{-2}), respectively. Core metals (Zn, Mn, Ag, Co, V, Ni) coupling with palladium atoms can change the outer electronic structure of palladium, which affects the energy involved in the adsorption/desorption of palladium to H_2O_2. In other words, the lattice strain and synergistic effects in the core−shell region can increase the utilization of metal atoms and result in changes in the electronic structure, which can significantly improve the catalyst activity and cause differences in the current densities. Among the catalysts prepared, the Zn@Pd/CNT catalyst showed the best activity in the H_2O_2 electro-reduction reaction with the highest peak current density. The consequences confirmed that the modification of GCE with highly conductive Zn@Pd/CNT modification to the GCE increased the electrode conduction and significantly improved the conductivity of the electrode. Subsequent experiments were carried out with the Zn@Pd/CNT catalyst.

The electro-reduction of H_2O_2 on the Zn@Pd/CNT-modified GCE has been investigated for different experimental conditions. First, the effect of the NaOH concentration was studied by cyclic voltammetry for various concentrations of NaOH and a 0.25 M H_2O_2 solution. Clearly, the NaOH concentration effect for H_2O_2 electro-reduction on the Zn@Pd/CNT-modified GCE is much more significant, as shown in Figure 6. The H_2O_2 electro-reduction current increases as the NaOH concentration increases up to 3.0 M.[3,35] The current density then decreases with a further increase in NaOH molarity until 5.0 M.[36] The increase in the NaOH concentration has no advantage for the improvement of hydrogen peroxide reduction; therefore, it is useless, and as a result, the optimum NaOH value is 3.0 M.

https://doi.org/10.1021/acsomega.3c05531
ACS Omega 2023, 8, 38577−38586

Table 1. Comparison of Different Catalysts for Electrochemical Reduction of H_2O_2

catalysts	electrolyte concentration NaOH (M)	H_2O_2 concentration (M)	potential (V)	current density (mA cm^{-2})	reference
$PdCoMn_2O_4$	3.0	0.7	− 0.80	580	8
$Pd@Co_3O_4$/Ti	3.0 (KOH)	0.4	− 0.40	145.8	14
Pd−Co_3O_4/ RGO@PI	2.0	0.5	− 0.80	962	17
Pd/rGO/NF	3.0	0.5	− 0.50	303	30
$Pd@SnO_2$/Ni	3.0	0.5	− 0.54	320	37
PRN (Pd/rGO/Ni)	2.0	0.5	− 0.60	450	38
Pd-CNT/Ni foam	3.0 (KOH)	0.4	− 0.80	323	39
CoPd@graphite	1.0	1.4	− 0.60	270	40
Co/Co_3O_4	3.0	0.5	− 0.40	425	41
$NiCo_2O_4$@Ni foam	3.0 (KOH)	0.4	− 0.60	330	42
Pt−Co NS@C sponge	3.0 (KOH)	1.5	− 0.50	353	43
NanoAg	1.0	0.125	− 0.15	23.92	44
Zn@Pd/CNT	3.0	0.5	− 0.30	835	this work

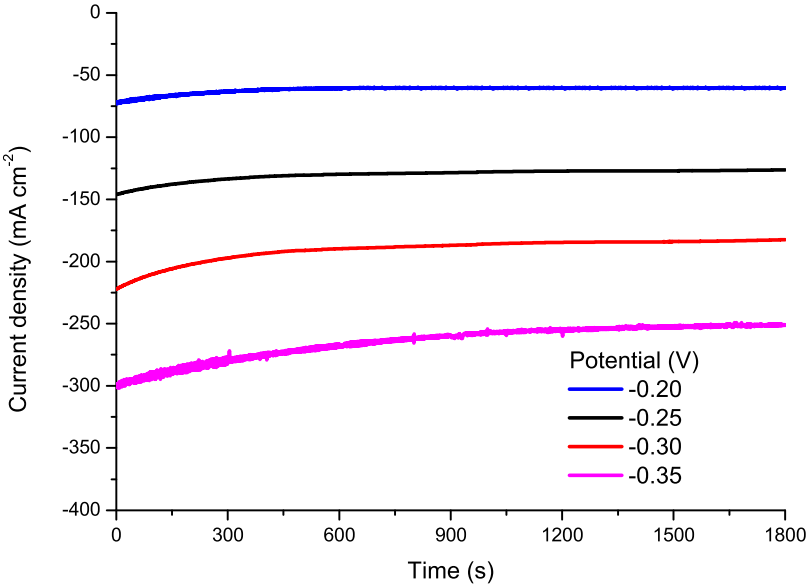

Figure 8. Chronoamperometric curves for H_2O_2 reduction on the Zn@Pd/CNT-modified GCEs in 3.0 M NaOH + 0.25 M H_2O_2 at different potentials.

The effect of H_2O_2 concentration on H_2O_2 electro-reduction was investigated with Zn@Pd/CNT-modified GCE. The cyclic voltammetric results of different concentrations of H_2O_2 are shown in Figure 7. Similar to NaOH, the electro-reduction current density on Zn@Pd/CNT-modified GCE also shows a remarkable increase with the change in H_2O_2 concentration. The peak current does not significantly increase when the H_2O_2 concentration is increased further, though. Given that H_2O_2 is known to be unstable in strong alkaline electrolytes, this tendency is likely caused by severe H_2O_2 chemical breakdown.[3,30]

Zn@Pd/CNT is an excellent catalyst for the reduction of hydrogen peroxide by comparison with other catalysts synthesized for the reduction of H_2O_2 in the literature.[8,14,30,37,38] By the evaluation of H_2O_2 electro-reduction on different modified electrodes in Table 1, the prepared Zn@Pd/CNT cathode catalyst displays a lower reduction potential and a higher current density than other reported cathode catalysts for H_2O_2 reduction.

Chronoamperometric studies were performed at various applied potentials to further demonstrate the performance of the Zn@Pd/CNT catalyst for H_2O_2 electro-reduction. The response of Zn@Pd/CNT-modified GCE at each potential increased significantly and reached a stable value in a short time after the test began as the potential went negative (Figure 8). The CA curves exhibit a gentle fluctuation when the potential is switched to a more negative value, which can be attributed to the disruption of the O_2 bubbles brought on by H_2O_2 breakdown.

EIS is a commonly used technique for exploring the charge transfer characteristics of the electrodes. At this point of the study, EIS was applied to explore the charge transfer resistance of electrodes modified with different catalysts. The typical Nyquist diagrams of M@Pd/CNT (M: Zn, Mn, Ag, Co, V, Ni)-modified GCEs obtained at −0.3 V are given in Figure 9. A single semicircle that is associated with the charge transfer resistance (Rct) at the solid−electrolyte interface can be seen in the high-frequency region. The Rct values of M@Pd/CNT (M: Zn, Mn, Ag, Co, V, Ni) and Pd/CNT catalysts are about 35, 73, 105, 157 and 200, 350 Ω, respectively. It appears that Zn@Pd/CNT has the smallest resistance at the catalyst−electrolyte interface, indicating that it would be better suited to serve as the cathode catalyst for a H_2O_2 fuel cell.

https://doi.org/10.1021/acsomega.3c05531
ACS Omega 2023, 8, 38577−38586

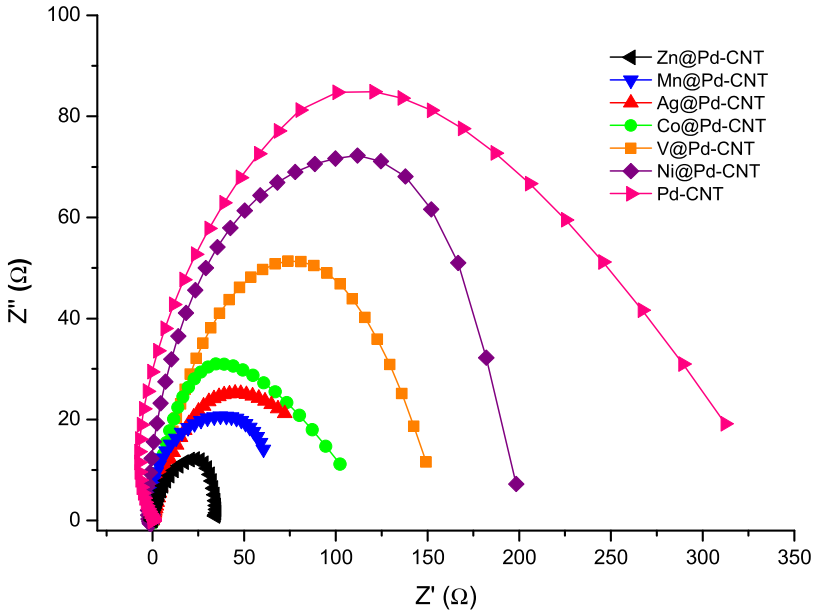

Figure 9. Nyquist plots of H_2O_2 electro-reduction on the M@Pd/CNT (M: Zn, Mn, Ag, Co, V, Ni)-modified GCEs at −0.3 V in 3.0 M NaOH +0.25 M H_2O_2.

4. CONCLUSIONS

Palladium-based catalysts were prepared on CNT by the sodium borahydrate reduction method. M@Pd/CNT (M: Zn, Mn, Ag, Co, V, Ni) electrocatalysts' activities toward H_2O_2 reduction in alkaline solution were evaluated using different electrochemical methods. The Zn@Pd/CNT catalyst has a current density of 273.2 mA cm^{-2}, which is 3.95 times higher than that of Pd/CNT catalyst-modified electrodes with respect to the CV results. The findings of CA curves further demonstrated that Zn@Pd/CNT has the highest steady-state current density for the H_2O_2 electro-reduction process among the synthesized electrocatalysts. Additionally, because Zn@Pd/CNT showed the lowest charge transfer resistance (35 Ω) compared to the other electrocatalysts, the findings of the EIS spectra confirmed the results of CV and CA. The results showed that Zn@Pd/CNT-modified GCE for the H_2O_2 electro-reduction reaction had excellent catalytic activity and stability, and it could be used as a catalyst.

AUTHOR INFORMATION

Corresponding Author

Ozlem Gokdogan Sahin − *Chemical Engineering Department, Konya Technical University, 42250 Konya, Turkey;* orcid.org/0000-0001-6188-5517; Email: osahin@ktun.edu.tr

Author

Burak Yapici − *Chemical Engineering Department, Konya Technical University, 42250 Konya, Turkey;* orcid.org/0000-0002-1244-2178

Complete contact information is available at: https://pubs.acs.org/10.1021/acsomega.3c05531

Notes

The authors declare no competing financial interest.

ACKNOWLEDGMENTS

The authors appreciate the scholarship (2210-C National MSc/MA Scholarship Program in the Priority Fields in Science and Technology) from the Scientific and Technological Research Council of Turkey (TUBITAK) and the financial support from Konya Technical University Scientific Research Projects Coordination (project no: 18201153).

REFERENCES

(1) Bagotsky, V. S.; Skundin, A. M.; Volfkovich, Y. M. *Electrochemical Power Sources: Batteries, Fuel Cells, and Supercapacitors*; John Wiley & Sons, 2015.

(2) Celik, C.; Boyaci San, F.; Sarac, H. Investigation of Ni foam effect for direct borohydride fuel cell. *Fuel Cells* **2012**, *12* (6), 1027−1031.

(3) Wang, Y.; Cheng, K.; Cao, D.; Yang, F.; Yan, P.; Zhang, W.; Wang, G. Preparation of NiCo2O4 nanosheet arrays and its high catalytic performance for H2O2 electroreduction. *Fuel Cells* **2015**, *15* (2), 298−305.

(4) Nadeem, M.; Yasin, G.; Arif, M.; Bhatti, M. H.; Sayin, K.; Mehmood, M.; Yunus, U.; Mehboob, S.; Ahmed, I.; Flörke, U. Pt-Ni@ PC900 hybrid derived from layered-structure Cd-MOF for fuel cell ORR activity. *ACS Omega* **2020**, *5* (5), 2123−2132.

(5) Song, C.; Wang, G.; Zhang, F.; Zhu, K.; Cheng, K.; Ye, K.; Yan, J.; Cao, D.; Yan, P. One-pot synthesis of crossed Fe2O3 nanosheets in-situ grown on Ni foam and the application for H2O2 electro-oxidation. *J. Alloys Compd.* **2020**, *817*, No. 152770.

(6) Wang, S.; Ye, D.; Liu, Z.; Zhu, X.; Chen, R.; Liao, Q.; Yang, Y.; Liu, H. A flexible on-fiber H2O2 microfluidic fuel cell with high power density. *Int. J. Hydrogen Energy* **2022**, *47* (7), 4793−4803.

(7) Xiao, X.; Yang, F.; Cheng, K.; Wang, X.; Zhang, H.; Ye, K.; Wang, G.; Cao, D. Enhanced performance of direct peroxide/peroxide fuel cell by using ultrafine Nickel Ferric Ferrocyanide nanoparticles as the cathode catalyst. *Int. J. Hydrogen Energy* **2017**, *42* (36), 22856−22865.

(8) Song, C.; Li, X.; Zhang, L.; Yan, P.; Xu, C.; Zhu, K.; Cheng, K.; Ye, K.; Yan, J.; Cao, D.; Wang, G. Pd nanoparticles anchored to nano-peony CoMn2O4 as an efficient catalyst for H2O2 electroreduction. *J. Electroanal. Chem.* **2020**, *858*, No. 113711.

(9) Han, L.; Guo, S.; Wang, P.; Dong, S. Light-Driven, Membraneless, Hydrogen Peroxide Based Fuel Cells. *Adv. Energy Mater.* **2015**, *5* (2), 1400424.
(10) An, J.; Li, N.; Zhao, Q.; Qiao, Y.; Wang, S.; Liao, C.; Zhou, L.; Li, T.; Wang, X.; Feng, Y. Highly efficient electro-generation of H2O2 by adjusting liquid-gas-solid three phase interfaces of porous carbonaceous cathode during oxygen reduction reaction. *Water Res.* **2019**, *164*, No. 114933.
(11) Song, C.; Li, B.; Ye, K.; Zhu, K.; Cao, D.; Cheng, K.; Wang, G.; Pan, Y. Investigation of palladium nanoparticles supported on metallic titanium pillars as a novel electrode for hydrogen peroxide electroreduction in acidic medium. *Electrochim. Acta* **2017**, *250*, 251−258.
(12) Kirubaharan, C. J.; Kumar, G. G.; Sha, C.; Zhou, D.; Yang, H.; Nahm, K. S.; Raj, B. S.; Zhang, Y.; Yong, Y.-C. Facile fabrication of Au@ polyaniline core-shell nanocomposite as efficient anodic catalyst for microbial fuel cells. *Electrochim. Acta* **2019**, *328*, No. 135136.
(13) Yang, F.; Cheng, K.; Wu, T.; Zhang, Y.; Yin, J.; Wang, G.; Cao, D. Dendritic palladium decorated with gold by potential pulse electrodeposition: Enhanced electrocatalytic activity for H2O2 electroreduction and electrooxidation. *Electrochim. Acta* **2013**, *99*, 54−61.
(14) Cheng, K.; Yang, F.; Xu, Y.; Cheng, L.; Bao, Y.; Cao, D.; Wang, G. Pd doped Co3O4 nanowire array as the H2O2 electroreduction catalyst. *J. Power Sources* **2013**, *240*, 442−447.
(15) Shim, J. H.; Kim, J.; Lee, C.; Lee, Y. Porous Pd layer-coated Au nanoparticles supported on carbon: synthesis and electrocatalytic activity for oxygen reduction in acid media. *Chem. Mater.* **2011**, *23* (21), 4694−4700.
(16) Yunphuttha, C.; Porntheeraphat, S.; Midpanon, S.; Wongchaisuwat, A.; Viravathana, P. Improving the catalytic activity of lanthanum manganese oxide with strontium doping for hydrogen peroxide reduction reaction in micro direct alcohol-hydrogen peroxide fuel cell. *J. Power Sources* **2018**, *392*, 251−259.
(17) Yang, M.; Zhang, C.; Zhao, J.; Wang, L.; Li, L.; Guo, S. Construction of free-standing electrode anchored on polyimide foam with a facile synergistic strategy for enhancing hydrogen peroxide reduction electrocatalysis. *J. Alloys Compd.* **2022**, *891*, No. 161939.
(18) Han, B.; Xu, C. Nanoporous PdFe alloy as highly active and durable electrocatalyst for oxygen reduction reaction. *Int. J. Hydrogen Energy* **2014**, *39* (32), 18247−18255.
(19) Kaur, A.; Kaur, G.; Singh, P. P.; Kaushal, S. Supported bimetallic nanoparticles as anode catalysts for direct methanol fuel cells: A review. *Int. J. Hydrogen Energy* **2021**, *46* (29), 15820−15849.
(20) Sun, L.; Shi, L.; Zhang, S.; He, W.; Zhang, Y. Cu-and Co-Modified Pd/C Nanoparticles as the High Performance Cathodic Catalysts for Mg-H2O2 Semi-Fuel Cell. *Fuel Cells* **2017**, *17* (6), 898−904.
(21) Yang, F.; Cheng, K.; Wu, T.; Zhang, Y.; Yin, J.; Wang, G.; Cao, D. Au−Pd nanoparticles supported on carbon fiber cloth as the electrocatalyst for H2O2 electroreduction in acid medium. *J. Power Sources* **2013**, *233*, 252−258.
(22) (a) Ding, X.; Yin, S.; An, K.; Luo, L.; Shi, N.; Qiang, Y.; Pasupathi, S.; Pollet, B. G.; Shen, P. K. FeN stabilized FeN@ Pt core−shell nanostructures for oxygen reduction reaction. *J. Mater. Chem. A* **2015**, *3* (8), 4462−4469. (b) Wang, C.-H.; Hsu, H.-C.; Wang, K.-C. Iridium-decorated Palladium−Platinum core−shell catalysts for oxygen reduction reaction in proton exchange membrane fuel cell. *J. Colloid Interface Sci.* **2014**, *427*, 91−97.
(23) Mahmoodi, R.; Hosseini, M. G.; Rasouli, H. Enhancement of output power density and performance of direct borohydride-hydrogen peroxide fuel cell using Ni-Pd core-shell nanoparticles on polymeric composite supports (rGO-PANI) as novel electrocatalysts. *Appl. Catal., B* **2019**, *251*, 37−48.
(24) Zhang, Y.; Han, T.; Fang, J.; Xu, P.; Li, X.; Xu, J.; Liu, C.-C. Integrated Pt 2 Ni alloy@ Pt core−shell nanoarchitectures with high electrocatalytic activity for oxygen reduction reaction. *J. Mater. Chem. A* **2014**, *2* (29), 11400−11407.
(25) Karuppannan, M.; Kim, Y.; Gok, S.; Lee, E.; Hwang, J. Y.; Jang, J.-H.; Cho, Y.-H.; Lim, T.; Sung, Y.-E.; Kwon, O. J. A highly durable carbon-nanofiber-supported Pt−C core−shell cathode catalyst for ultra-low Pt loading proton exchange membrane fuel cells: facile carbon encapsulation. *Energy Environ. Sci.* **2019**, *12* (9), 2820−2829.
(26) Kim, T.; Kwon, Y.; Kwon, S.; Seo, J. G. Substrate effect of platinum-decorated carbon on enhanced hydrogen oxidation in PEMFC. *ACS Omega* **2020**, *5* (41), 26902−26907.
(27) Lam, E.; Luong, J. H. Carbon materials as catalyst supports and catalysts in the transformation of biomass to fuels and chemicals. *ACS Catal.* **2014**, *4* (10), 3393−3410.
(28) Fujigaya, T.; Nakashima, N. Fuel cell electrocatalyst using polybenzimidazole-modified carbon nanotubes as support materials. *Adv. Mater.* **2013**, *25* (12), 1666−1681.
(29) (a) Endo, M.; Iijima, S.; Dresselhaus, M. S. *Carbon Nanotubes*; Elsevier, 2013. (b) Li, L.; Xing, Y. Electrochemical durability of carbon nanotubes at 80 C. *J. Power Sources* **2008**, *178* (1), 75−79.
(30) Sun, L.; Wen, F.; Li, S.; Zhang, Z. High efficient rGO-modified Ni foam supported Pd nanoparticles (PRNF) composite synthesized using spontaneous reduction for hydrogen peroxide electroreduction and electrooxidation. *J. Power Sources* **2021**, *481*, No. 228878.
(31) Hosseini, M. G.; Daneshvari-Esfahlan, V.; Aghajani, H.; Wolf, S.; Hacker, V. Palladium-nickel electrocatalysts on nitrogen-doped reduced graphene oxide nanosheets for direct hydrazine/hydrogen peroxide fuel cells. *Catalysts* **2021**, *11* (11), 1372.
(32) Pinheiro, V. S.; Souza, F. M.; Gentil, T. C.; Parreira, L. S.; Batista, B. L.; Santos, M. C. Hybrid palladium-ceria nanorod electrocatalysts applications in oxygen reduction and ethanol oxidation reactions in alkaline media. *Int. J. Hydrogen Energy* **2021**, *46* (29), 15896−15911.
(33) Cui, X.; Li, Y.; Zhao, M.; Xu, Y.; Chen, L.; Yang, S.; Wang, Y. Facile growth of ultra-small Pd nanoparticles on zeolite-templated mesocellular graphene foam for enhanced alcohol electrooxidation. *Nano Res.* **2019**, *12* (2), 351−356.
(34) Yang, Y.; Xue, Y.; Huang, F.; Zhang, H.; Tao, K.; Zhang, R.; Shen, Q.; Chang, H. A facile microfluidic hydrogen peroxide fuel cell with high performance: electrode interface and power-generation properties. *ACS Appl. Energy Mater.* **2018**, *1* (10), 5328−5335.
(35) Xue, Y.; Cai, W.; Zheng, S.; Yan, W.; Hu, J.; Sun, Z.; Zhang, Y.; Jin, W. W-doped MoS 2 nanosheets as a highly-efficient catalyst for hydrogen peroxide electroreduction in alkaline media. *Catal. Sci. Technol.* **2017**, *7* (23), 5733−5740.
(36) Sun, L.; Li, S.; Zhang, N.; Xu, X.; Shi, L.; Zhang, Y.; Song, Y. Spider chrysanthemum-like Co flowers on a Ni foam for highly efficient H2O2 electroreduction in alkaline media. *J. Alloys Compd.* **2023**, *932*, No. 167720.
(37) Sun, L.; He, W.; Li, S.; Shi, L.; Zhang, Y.; Liu, J. The high performance mushroom-like Pd@ SnO2/Ni foam electrode for H2O2 reduction in alkaline media. *J. Power Sources* **2018**, *395*, 386−394.
(38) Song, C.; Cao, L.; Li, B.; Huang, X.; Ye, K.; Zhu, K.; Cao, D.; Cheng, K.; Wang, G. Highly efficient palladium nanoparticles decorated reduced graphene oxide sheets supported on nickel foam for hydrogen peroxide electroreduction. *Appl. Surf. Sci.* **2017**, *426*, 1046−1054.
(39) Yang, F.; Cao, B.; Tao, Y.; Hu, M.; Feng, C.; Wang, L.; Jiang, Z.; Cao, D.; Zhang, Y. Electrodeposition of palladium on carbon nanotubes modified nickel foam as an efficient electrocatalyst towards hydrogen peroxide reduction. *J. Power Sources* **2015**, *298*, 38−45.
(40) Zhang, D.; Ye, K.; Cao, D.; Yin, J.; Cheng, K.; Wang, B.; Xu, Y.; Wang, G. Catalytic behavior of a palladium doped binder free paper based cobalt electrode in electroreduction of hydrogen peroxide. *J. Power Sources* **2015**, *273*, 1142−1147.
(41) Song, C.; Zhang, D.; Ye, K.; Zeng, W.; Yang, X.; Wang, Y.; Shen, Y.; Cao, D.; Cheng, K.; Wang, G. In-situ reduced petal-like cobalt on Ni foam based cobaltosic oxide as an efficient catalyst for hydrogen peroxide electroreduction. *J. Electroanal. Chem.* **2017**, *788*, 74−82.
(42) Xiao, X.; Yang, F.; Cheng, K.; Wang, X.; Yin, J.; Ye, K.; Wang, G.; Cao, D. NiCo2O4 nanostructures with various morphologies as

https://doi.org/10.1021/acsomega.3c05531
ACS Omega 2023, 8, 38577−38586

the high-performance electrocatalysts for H2O2 electroreduction and electrooxidation. *J. Electroanal. Chem.* **2014**, *729*, 103−108.
(43) Ye, K.; Zhang, D.; Zhang, H.; Cheng, K.; Wang, G.; Cao, D. Platinum-modified cobalt nanosheets supported on three-dimensional carbon sponge as a high-performance catalyst for hydrogen peroxide electroreduction. *Electrochim. Acta* **2015**, *178*, 270−279.
(44) Yi, Q.; Niu, F.; Li, L.; Du, R.; Zhou, Z.; Liu, X. Novel nanoporous silver particles for electro-reduction of hydrogen peroxide in alkaline media. *J. Electroanal. Chem.* **2011**, *654* (1−2), 60−65.

https://doi.org/10.1021/acsomega.3c05531
ACS Omega 2023, 8, 38577−38586